Silicon (2023) 15:897–912
https://doi.org/10.1007/s12633-022-02061-3

Dry Sliding Wear Behavior of Tempered (T4 and T6) Hypereutectic Aluminum Alloy-Based Composites

Varun Singhal[1,2] · Aayush Gupta[3,4] · Om Prakash Pandey[1,4]

Received: 8 February 2022 / Accepted: 8 August 2022 / Published online: 23 August 2022

Abstract
The present work describes the effect of tempering (T4 and T6) processes on the dry sliding wear properties of ilmenite reinforced aluminum alloy (LM30) composites, prepared through stir casting route. In this process the composites were heated to 540 °C for 0.5–2 h followed by water quenching. Then the samples were first given (a) T4 treatment (natural ageing at room temperature), and in second case (b) T6 treatment (aged at 180 and 250 °C for 4 h before air cooling). Optical microscopy revealed the homogeneous distribution of ilmenite particles and redistributed silicon around the ilmenite in the alloy matrix. Rockwell hardness values suggested the superiority of T6 treated composite samples as compared to T4 treated and untreated samples due to enhanced precipitation of intermetallic compounds viz. $Al_{13}Fe_4$, $FeSn_2$, FeTiSi, and Al_3Ti. Similarly, superior wear resistance (against steel disc) of T6 treated composite samples was also observed. A responsible mechanism has also been established with the help of scanning electron microscopy of worn surface and wear debris. Finally, a comparative study revealed the excellent (~4.0%) wear resistance (against EN31 steel disc) of T6 treated composite sample as compared to grey cast iron (traditional material) for brake drum applications.

Keywords Hypereutectic alloy · Ilmenite · Wear rate · Heat treatment · Dry sliding wear

1 Introduction

Ceramic reinforced aluminum composites (AMCs) with high specific strength, elastic modulus, stiffness, and wear resistance have a wide range of applications in the transportation sectors, including automobiles and aviation [1–3]. Such attractive features of AMCs are introduced by the appropriate dispersion of ceramic phase in the ductile Al metal or its alloy which is considered as the most critical parameter to obtain overall desired performance. However, one of the vital drawbacks of these composites is their low formability, caused by the brittle particles and their bonding with metallic matrix (i.e., weak interface). Liquid metallurgical route i.e., stir casting provides a better homogeneity of reinforced particles in metallic matrix at low cost which enabled it as one of the most promising and commercial methodology for developing AMCs [2, 4]. Due to excellent flowability and ability to form intermetallic compounds, hypereutectic Al-Si alloys (Si < 12.6 wt.%) can be employed as matrix material to fabricate AMCs with superior mechanical properties, corrosion resistance, abrasion resistance, and low thermal expansion as compared to hypoeutectic Al-Si alloys [5]. However, the size of primary Si and eutectic Al-Si mixture would also play a vital role in improving the overall characteristics of these alloys like LM30 [6, 7].

Despite of excellent mechanical properties, Al-alloys lack in heat treatment competency. Thus, Mg has been added to the Al-Si matrix introducing Mg_2Si precipitates (age hardening) which are responsible for material strengthening with enhanced stiffness [8]. Similarly, the addition of Cu (0.5–2.0 wt.%) increases the heating capacity of Al-alloy and led to form AlCu compounds improving the material's strength [9]. It is well-accepted that the heat treatment process improves the material properties significantly. The

✉ Om Prakash Pandey
oppandey@thapar.edu

1 Metallurgical Lab, Thapar Institute of Engineering and Technology, Patiala 147004, India

2 Department of Mechanical Engineering, IMS Engineering College, Ghaziabad 201001, India

3 Department of Mechanical Engineering, GLA University, Mathura 281406, India

4 Functional Materials Lab, Thapar Institute of Engineering and Technology, Patiala 147004, India

inclusion of other alloying elements, ceramic reinforcement and the associated heat treatment regulate the chemistry of the alloy and composite as well [6, 10].

Several research groups also reported the use of natural minerals e.g., sillimanite [11], rutile [12], garnet [13], and zircon [14] as alternate reinforcement material to synthetic ceramic particles (SiC, B_4C, CNTs etc.). These minerals help to improve the overall hardness, wear resistance, and thermal properties of the AMCs [11, 15, 16]. Karthikeyan et al. [17] have reported that the material becomes more ductile with refined grain size leading to reduction in the wear rate and coefficient of friction (COF) of the composite. Moreover, the strong interfacial bonding between matrix and reinforcement also provides an improvement in wear properties of the composites. Mann et al. [18] concluded that the wear resistance of AMC was increased by the incorporation of corundum particles. In the same sequence, authors have also reported that the Si morphology was refined in dual range particle sizes reinforced composites than the single range particle size. The wear resistance properties were also more than the single range reinforced composites.

Among these natural minerals, ilmenite exhibits high strength, corrosive resistance and crystalline iron titanium oxide ($FeTiO_3$) with 4.7 gm/cc. It is mainly found along the seashores of Orissa and Tamil Nadu in Indian subcontinent. As per the report of Rasidhar et al. [19] and Elwan et al. [20], the addition of $FeTiO_3$ mineral into the Al-Si alloy enhanced the mechanical properties of AMCs. $FeTiO_3$ forms a secondary phase i.e., $FeAl_3$, which restricts the dislocation development and its motion inside the Al-matrix and provide more resistance to applied loads. Arora et al. [12] and Kumar et al. [21] observed that rutile (TiO_2) mineral (as reinforcement) improves the wear resistance of produced AMCs by refining the Si phase existing in the Al-Si base alloy.

Moreover, to overcome wear and friction losses, solid lubricants (graphite (Gr), tin (Sn), lead (Pb), and molybdenum disulfide (MoS_2), etc.) have also been incorporated in AMCs [22, 23]. In our earlier findings, the addition of solid lubricant (0.5 wt.% Sn-0.5 wt.% Gr) along with 10 wt.% ilmenite in the LM30 alloy exhibited better wear resistance as compared to non-lubricated AMCs under different loading conditions [24]. Shanmugaselvam et al. [25] synthesized the AMCs by adding the reinforcement $SiC + B_4C + Gr$ (2, 4, 6 wt.%) in the LM30 Al-Si alloy matrix. They suggested that stir casting has led to higher wear resistance with more hardness because it helped to disperse the particles homogeneously all over the matrix.

In the present work, solid lubricants (Sn/Gr) and ilmenite particles have been reinforced in the matrix of LM30 (Al-alloy) and heat treatment processes (T4 and T6) were performed. Here, primary goal of an aging treatment (T4 or T6) is to have precipitation of intermetallic phases in the alloy matrix, which can provide strengthening mechanism to the developed composites. Moreover, the heat treatment of Al-Si alloys leads to the improvement in the wear properties of the composites. For example, Sharma et al. [26] observed that the T4 and T6 heat treatment processes refined the eutectic and primary silicon morphology compared to untreated samples. The wear rate of composites was reduced because of heat treatment. Chen et al. [27] and Lashgari et al. [28] observed the enhanced wear resistance of A356-SiC and A356-B_4C composites with T6 heat treatment as compared to non-heat treated AMCs. In the present investigation, the wear behavior was investigated and compared to that of cast iron, used in the automotive industry as brake drums. Finally, SEM–EDS analysis of worn surface/debris established a link between wear outcomes and involved mechanism.

2 Experimental

2.1 Material and Method

For the fabrication of AMCs, hypereutectic LM30 Al-Si alloy (Al-76.48 wt.%, Si-17.74 wt.%, Cu-4.09 wt.%; EMPL, India), ilmenite minerals (TiO_2-55.3 wt.%, FeO-20.5 wt.%, Fe_2O_3-19.9 wt.%; IREL, India) and cast iron (Fe-93.77 wt.%, C-3.52 wt.%, Si-1.66 wt.%) were used. The compositional details of LM30 alloy, ilmenite, and cast iron are well in-line with earlier studies [11, 16, 29]. The detailed steps followed for composite preparation are already reported in an earlier work as shown in Fig. 1a [11, 16]. The adopted heat treatment process is shown in Fig. 1b where the effect of holding time during quenching and artificial ageing at 180 and 250 ºC temperature as per the ASM metal handbook [30] has been observed with small time interval to understand structural modifications for dry sliding wear applications. Table 1 contains information about the samples.

2.2 Characterization

Initially, to investigate the distribution of ilmenite particles inside the Al-matrix, samples were prepared by the metallographic procedure as per the ASTM E3-11. The prepared samples were examined under the optical microscope (Eclipse MA-100, Tokyo, Japan). Heat treatment was done in resistance heating furnace. X-ray diffraction technique was used to identify different phases present in the samples. The X-ray diffraction was recorded on PANanalytical X-pert Pro using Cu-Kα radiation ($\lambda = 1.5406$ Å, Ni filter) in the range of $20° \leq 2\theta \leq 80°$ (step size = 0.013°). The XRD pattern was matched with ICDD standard cards using X-pert High Score software as given in Table 2.

The hardness of samples was measured using Rockwell hardness tester, model no. TRSND (India). The tribometer (Wear and Friction Monitor TR-20, Ducom Instruments,

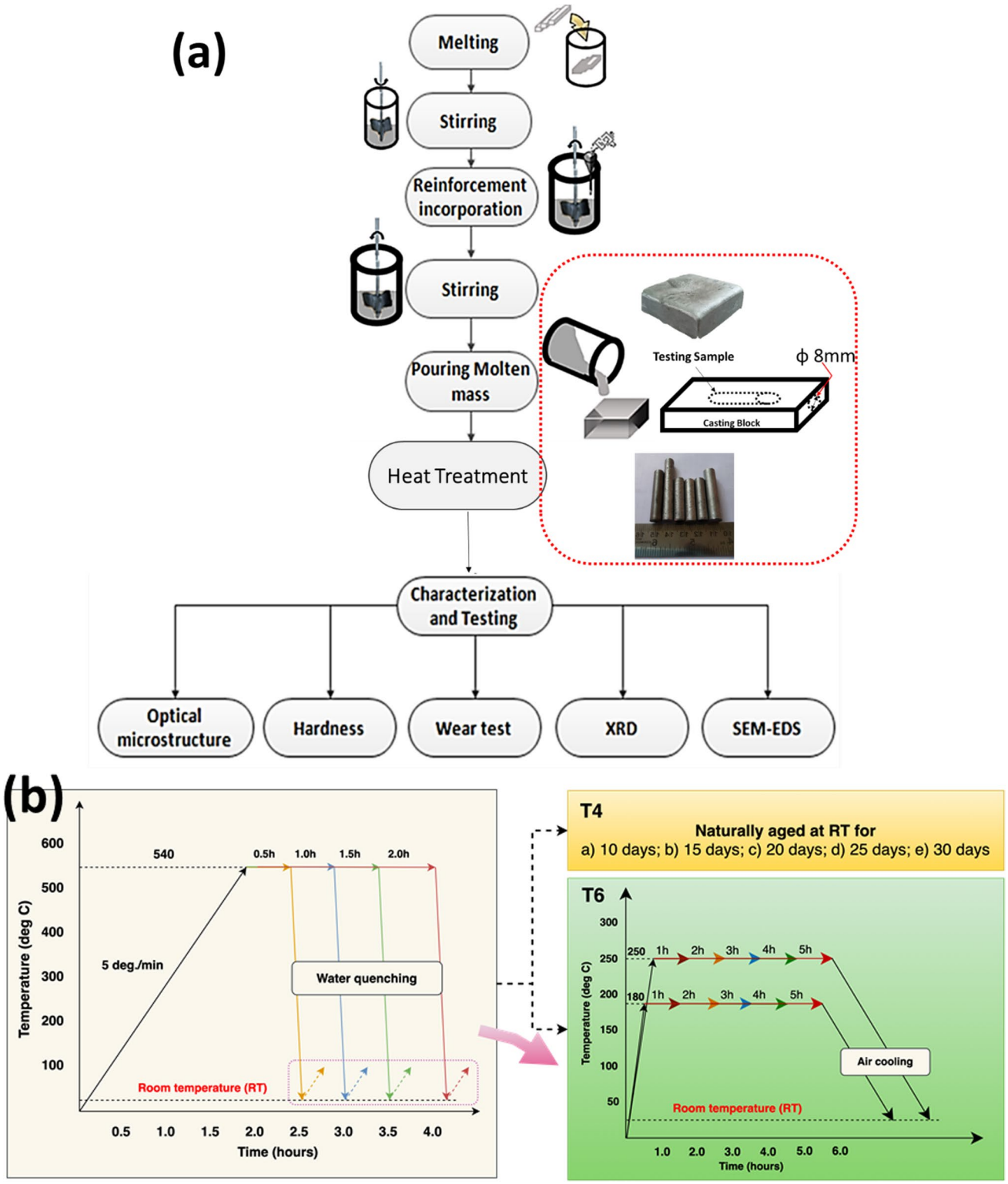

Fig. 1 (**a**) Flow diagram of preparation of AMCs samples and (**b**) detailed heat treatment cycle for the preparation of tempered AMCs

Bangalore, India) was used for wear measurement using pin-on-disc dry sliding wear test. Table 3 represents the details of the wear rate testing conditions [31, 32]. Further, the total wear loss of the sample in terms of volume is determined using $V_T = H_w \times A_I$ (V_T; wear loss, H_W; loss of height, A_I; area of contact ($= \frac{\pi}{4}d^2$), d

Table 1 Details and designations of different composite formulations

Sample	Amount (wt. %)			Heat treatment
	Ilmenite	Sn	Gr	
LM30	-	-	-	-
LM30-T4				(540 °C + 1 h) → water quench → T4 (20 days at room temperature (RT))
LM30-T6				(540 °C + 1 h) → water quench → T6 (180 °C + 4 h → air cool)
LM30-T6/1				(540 °C + 1 h) → water quench → T6 (250 °C + 4 h → air cool)
ITG10	10	-	-	-
ITG10-T4	10	0.5	0.5	(540 °C + 1 h) → water quench → T4 (20 days at room temperature (RT))
ITG10-T6	10	0.5	0.5	(540 °C + 1 h) → water quench → T6 (180 °C + 4 h → air cool)
ITG10-T6/1	10	0.5	0.5	(540 °C + 1 h) → water quench → T6 (250 °C + 4 h → air cool)

pin diameter). The height loss was measured from the attached LVDT sensor in the tribometer. In addition, the wear was determined by using; $W_r = \frac{V_T}{D}$; W_r – wear rate, D – sliding distance (1.6 × time), and (COF) = $\frac{F}{L}$; (F – Friction force, L – Normal load). Raw data was averaged on 3 consecutive runs for 4 different samples (total 12 data points) with same composition under same conditions. JOEL scanning electron microscope (JSM-6510LV, Tokyo, Japan) was used to analyze the worn surface and debris to understand the wear mechanism.

3 Results and Discussion

The study was carried out in continuation of previous work which elaborated the effect of different amount of ilmenite and solid lubrication on tribological performance of LM30 alloy [24]. From that earlier work, sample ITG10 (10% ilmenite + 0.5% Sn + 0.5% Gr) exhibited superior dry sliding wear resistance than non-reinforced and non-lubricated samples. Therefore, same sample was further used to understand the effect of tempering (T4 and T6) on wear performance of ilmenite reinforced LM30 lubricated composite.

Table 2 Details of ICDD cards used in phase analysis

Constituents	Chemical Formulae	Sign	ICDD card
Aluminum	Al	α	01–089-3657
Silicon	Si	γ	01–089-5012
Ilmenite	$FeTiO_3$	I	01–073-2233
Iron tin	$FeSn_2$	*	01–073-2030
Aluminum titanium	Al_3Ti	ξ	03–065-4505
Aluminum copper	Al_2Cu	β	01–089-1981
Aluminum iron	$Al_{13}Fe_4$	ε	00–050-0797
Titanium iron silicon	FeTiSi	•	01–088-2055
Magnesium silicon	Mg_2Si	◆	01–075-0445

3.1 Optical Microscopy

Figure 2(a, b) represents the optical microstructure of non-heat treated ITG10 composite containing 10 wt.% ilmenite with solid lubricants (0.5% Sn + 0.5% Gr). Figure 2a (at 100x) showcased the homogeneous distribution of ilmenite particles and eutectic-Si throughout the Al matrix. Here, mechanical stirring created a dynamic shear force in the melt, preventing ceramic particles from sinking and keeping them afloat [33]. Ilmenite has lesser specific thermal conductivity than Al-Si alloy stipulating nucleation sites for Si refinement to needle shaped primary Si from larger faceted Si which has been clearly demonstrated in Fig. 2b [34]. Similar observation, as an effect of ceramic reinforcement in Al-alloy matrix, has also been reported by our research group [35, 36].

After-T4 heat treatment, the morphology of eutectic-Si gets modified to spherical shape and needle-like morphology, as shown in Fig. 2(c, d). Moreover, the size of primary-Si has also been refined as compared to non-heat-treated sample, as shown in Fig. 2b. Figure 2(e, f) represents the optical micrograph of T6 treated composite sample. It revealed the morphological transformation of eutectic Si to globular shape which might be associated to the decreased surface energy of globular Si than its acicular shape. T6 treated composite sample contained the refined and uniform distribution of Si phase as compared to other heat-treated and untreated samples. The refined size of

Table 3 Details of operational parameters adopted for wear testing

Parameters	Details
Applied normal forces	9.81, 29.43, 49.05, and 68.67 N
Sliding velocity	1.6 m/sec
Test interval	32 min
Counter disc	EN31 die steel; 831 HV
Track diameter	100 mm
Pin diameter	8 mm
Standard	ASTM standard G99-05 (2010)
Sliding distance	3000 m

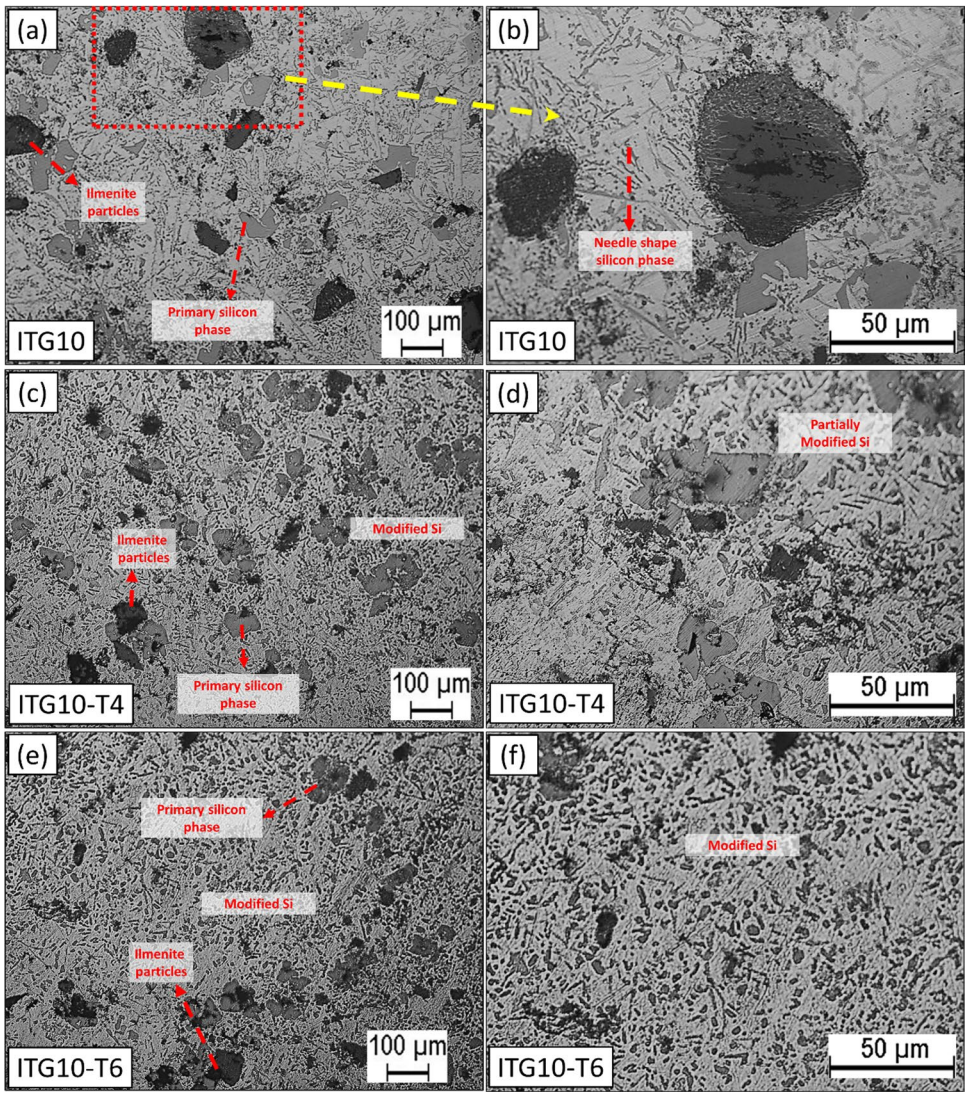

Fig. 2 Optical microstructure of ITG composite (**a**; 100X, **b**; 500X) non-heat treated, (**c**; 100X, **d**; 500X) T4 heat-treated, (**e**; 100X, **f**; 500X) T6 heat-treated

homogeneously distributed Si may help to enhance the bulk hardness of the composite and hence wear resistance of the composites [37, 38].

3.2 XRD and SEM Analysis

Figure 3(a, b) represents the XRD diffraction pattern and SEM–EDS analysis of ITG10 composite heat treatment at 540 °C for 1.0 h followed by water quenching in water and subsequently, artificially aged at 180 °C for 4.0 h and followed by air cooling. The XRD pattern, shown in Fig. 3a, demonstrated the presence of Al, Si, and ilmenite as major components of the prepared composite, while minor diffraction peaks represented the presence of intermetallic compounds such as FeTiSi, $Al_{13}Fe_4$, Fe_3Sn_5, Al_3Ti, Mg_2Si, and Al_2Cu because of tempering (T6). These phases are associated to chemical reactions between the particle–matrix during the heat treatment process. The room temperature aging process (T4) was insufficient to develop any of such intermetallic phases. While, a very long period for the natural ageing (12.0 h) process resulted to the development of Mg_2Si and Al_2Cu phases inside matrix [39]. Therefore, a period of 10–30 days was employed to understand the effect of natural aging. Since, heat treatment is used to facilitate the dispersion of alloying components, it results to the formation of a solid solution with the highest degree of super saturation. These precipitates are of Mg_2Si and Al_2Cu phases in the α-Al matrix. These intermetallic compounds and precipitates helped to improve the strength of samples [40–42]. In the Al-matrix, the major alloying elements are Al, Si, Cu, and Mg, which are partially dissolved in the α-Al solid solution and formed intermetallic phases with aluminum or among themselves which can be inferred from Fig. 3b.

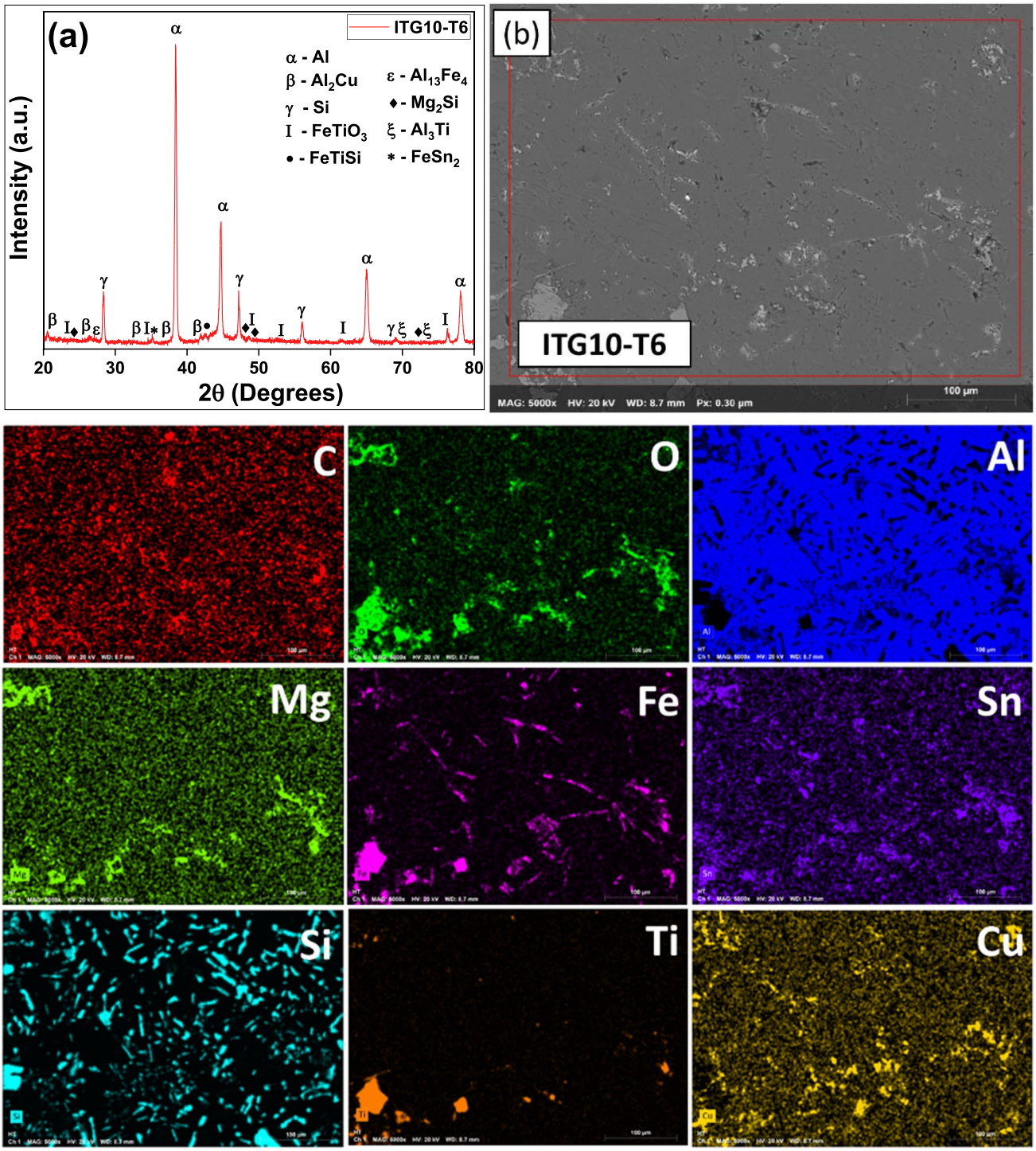

Fig. 3 (**a**) XRD of ITG10-T6, and SEM–EDS analysis of (**b**) ITG10-T6 and (**c**) ITG10-T4 composite

3.3 Hardness

Rockwell hardness testing was performed to determine the influence of heat treatment on the hardness of AMC samples. As-cast ITG10 sample exhibited ~ 91 HRB hardness which was reduced as an effect of quenching from 540 ºC, shown in Fig. 4a. Here, it was worth to note that increasing holding time before water quenching has reduced the effective hardness of the sample which might be associated to the dissolution of alloying element(s) in Al-matrix.

After the quenching of the composite samples, all four samples were aged for 10, 15, 20, 25, and 30 days under

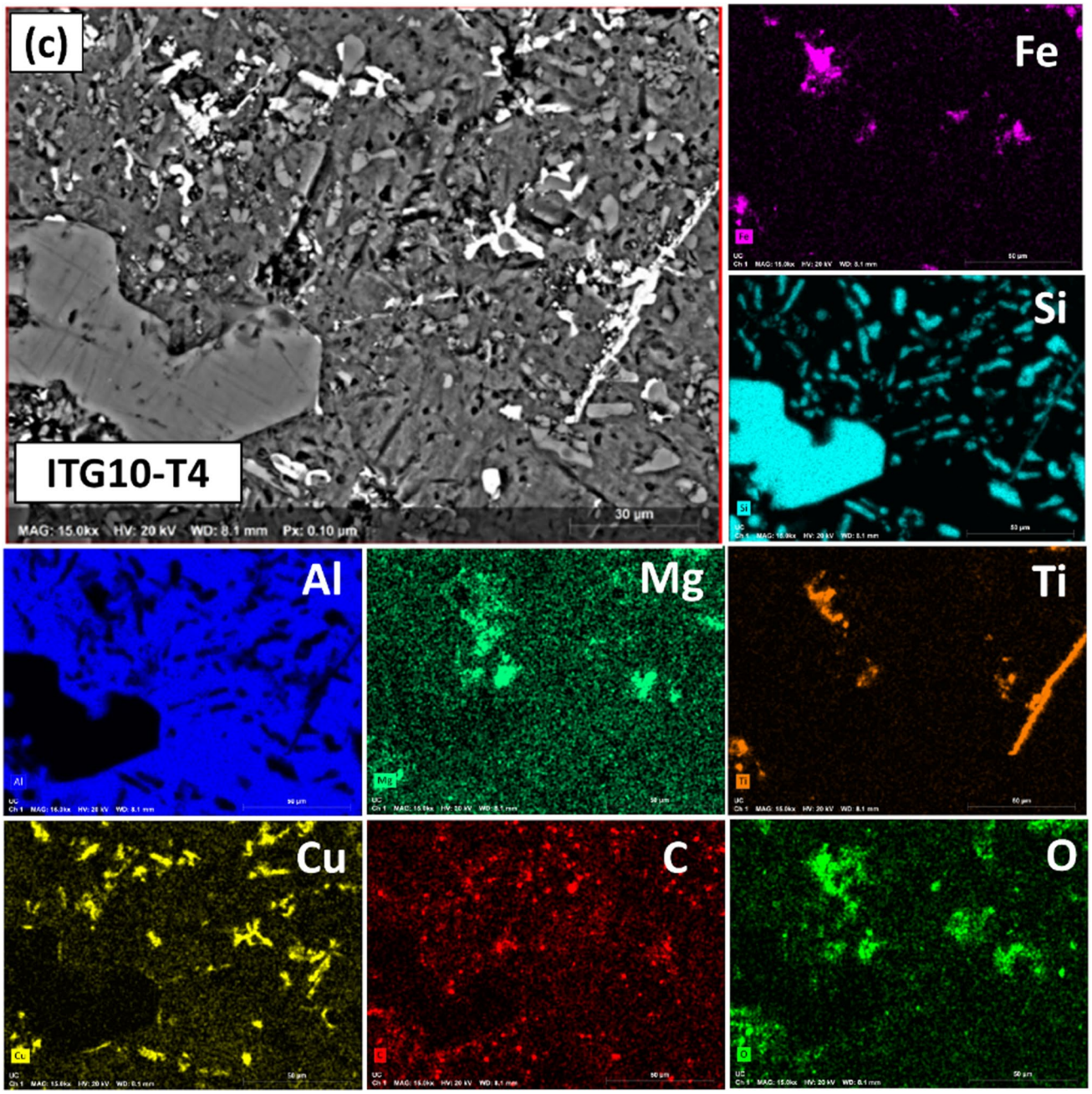

Fig. 3 (continued)

ambient conditions and hardness was measured which is shown in Fig. 4b. Here, as an effect of ageing process at ambient conditions i.e., T4 treatment, maximum hardness (112 ± 6 HRB) was observed for the ITG10 sample kept for 1.0 h at 540 ºC. It was clearly observed that hardness of the samples modified with respect to ageing time. All the quenched samples exhibited similar trend of hardness variation in which 20 days of ageing resulted to maximum increment in hardness. However, the hardness remained consistent beyond this point (i.e., 25 and 30 days). One more critical observation is related to the relative increment in hardness of the sample with respect to holding time before water quenching. Lesser holding time could efficiently increase the hardness of composite as compared to longer holding time before water quenching as shown in Fig. 4b.

Figure 5 depicts the effect of tempering (T6) treatment on the hardness of quenched ITG10 sample, aged at 180 °C (Fig. 5a) and 250 °C (Fig. 5b) for 1–5 h. The highest hardness was recorded for the artificially aged

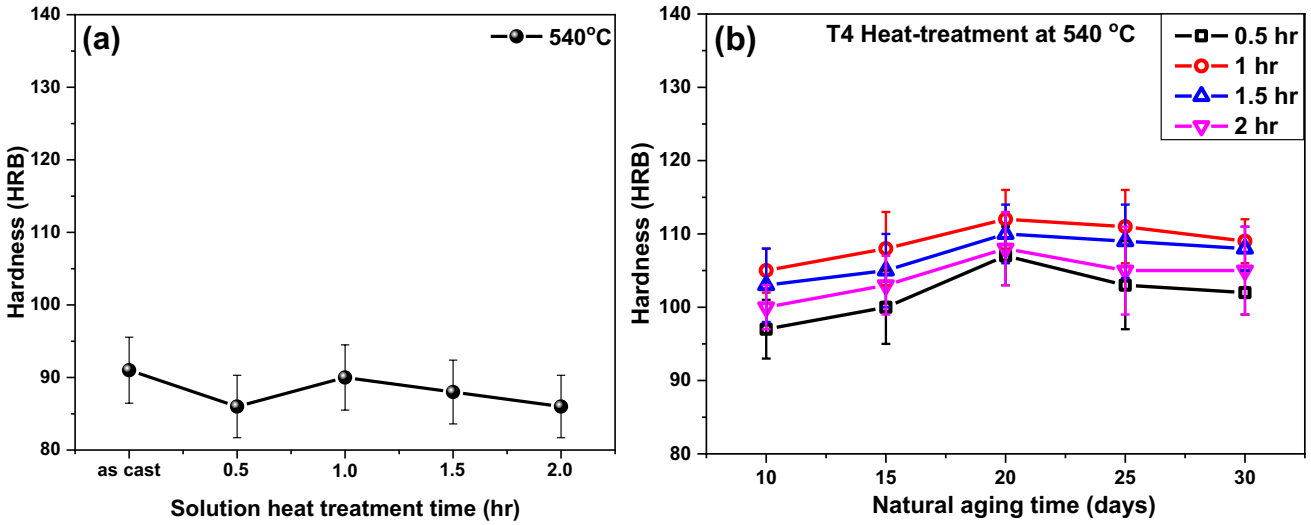

Fig. 4 Hardness variation (**a**) After solution heat treatment at different time (**b**) T4 heat-treated samples naturally aged 10, 15, 20, 25, and 30 days

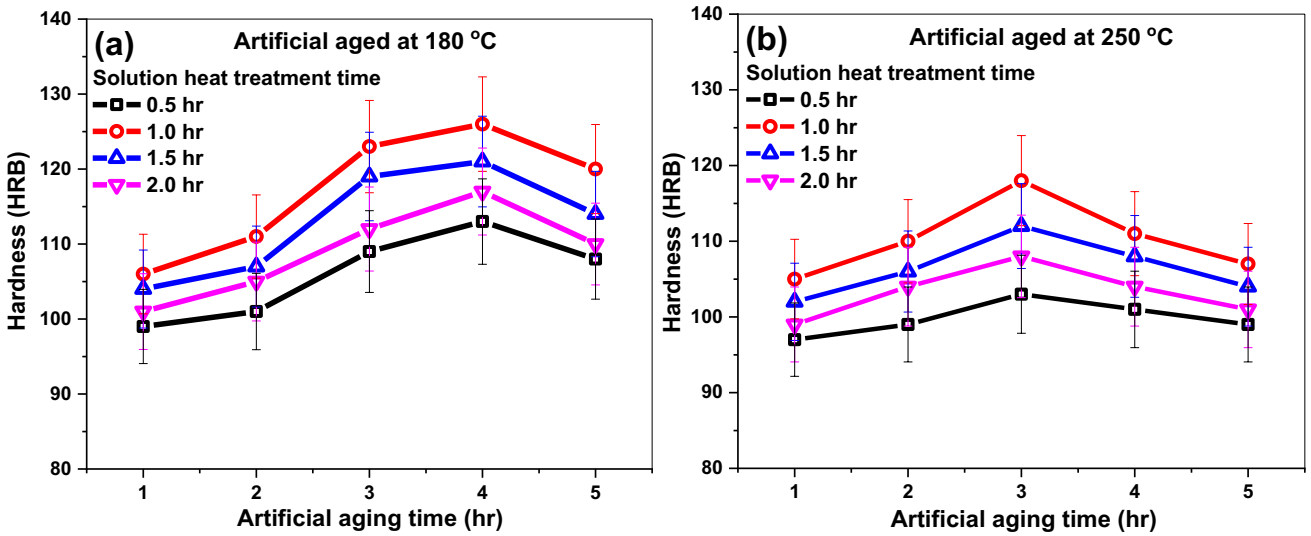

Fig. 5 Hardness of T6 heat-treated ITG10 sample aged for 1–5 h at (**a**) 180, and (**b**) 250 °C

samples at 180 °C after 4 h and at 250 °C after 3 h (respectively) of ageing. Increasing the ageing period beyond 4 h (at 180 °C) and 3 h (at 250 °C) reduces the hardness of the composites. The composite was heated between the 140–250 °C aiming to redistribute Al, Si Cu, and Mg and produce Mg_2Si and Al_2Cu precipitates [39]. These precipitates contribute to hardening of material through dislocation generation and annihilation. It has been observed that hardening process is accelerated with increasing ageing temperature as represented by Fig. 5 [43]. Higher ageing temperature facilitates the dislocations mobility and provides an accessible channel for diffusion of alloying elements. However, the dislocation around the particles does not migrate during the aging process but rather re-adjusts itself with time. Because the kinetics of diffusion is so slow, dislocations affect the normal ageing process [44]. The T6 heat-treated composites showed higher hardness than T4 heat-treated composites which might due to precipitation hardening (Mg_2Si and Al_2Cu).

3.4 Wear Testing

Since ITG10-T4 and ITG10-T6 samples exhibited the highest hardness in their respective categories therefore, these samples were used for dry sliding wear study to compare the wear behavior with the alloy i.e., LM30 as

shown in Fig. 6(a-c). The wear rate vs. sliding distance curve of non-heat treated, T4 heat treated (aged for 20 days; ITG10-T4) and T6 heat-treated (aged at 180 °C; ITG10-T6) samples are presented in Fig. 6 at (9.81–68.67 N) applied load. The study of these curves is based on two distinct areas (i) run-in wear, and (ii) steady-state wear. As per the visual observation, in the run-in wear area, the wear rate sharply increased to 250 m. After that, the wear rate declined rapidly up to 1750 and 1500 m for LM30 and AMCs, respectively. The interaction of surface asperities with the counter surface causes a dramatic increase in wear rate. The asperities on the hard counter surface tear the soft surface of the pin, resulting in abrasion on the pin surface which is termed as ploughing action. The pin surface asperities deform with a continuous sliding motion, resulting to the formation of abrasive grooves on the pin's surface. However, the resultant contact area between pin and counter surface has been increased and due to frictional energy, the contact surfaces were partially welded together. These welded zone was plastically deformed by the action of shear force and trigger the nucleation of cracks and ripping action in the form of severe material losses [33, 45].

While ilmenite reinforced composite (ITG10) exhibited reduced wear loss because ilmenite particles (being harder component) inhibited fracture growth and reduce the tearing of pin surface. Simultaneously, the thermal oxidation of metallic constituents occurs, and the development of hard oxide has been evidenced which further reduces the wear loss through oxidation wear mechanism [46, 47]. Hence, the wear rate of LM30 and ITG10 becomes steady, called steady-state wear as shown in Fig. 6a and d. The protective layer decreased the resultant contact area between the contact surfaces and the formation-deformation of protective oxide layer remains constant as a function of applied load and sliding motion. The presence of solid lubricants has already been discussed in earlier report [24]. The solid lubricant e.g., Sn initiates the formation of an intermetallic brittle phase $FeSn_2$ [48]. This lubricating film acts as a barrier between the counter surface asperities [49, 50]. Hence, decreased the shear stresses between contact surfaces which enhances galling [51] and seizure resistance [52]. This demonstrates the immediate improvement in composite material for anti-friction and anti-wear performance [53, 54].

Heat treated samples exhibited better wear resistance than non-treated samples. The maximum improvement in wear resistance was observed for ITG10-T4 and ITG10-T6 samples as shown in Fig. 6(c-f). Such observations reflect the contribution of Mg_2Si and Al_2Cu in hardening of the sample, which further reduced the wear loss. The other intermetallic compounds $Al_{13}Fe_4$, $FeSn_2$, FeTiSi and Al_3Ti in T6 heat treated composite (ITG10-T6) also contributed to the wear loss reduction due to the refined microstructure, dislocation annihilation [26, 55–57].

Wear study of heat-treated samples (alloy and composites) followed the similar trend that was obtained for hardness as observed from Fig. 7(a). Further, from the industrial point of view, a comparative study of the wear behavior has also been carried out for the prepared composites and cast iron as shown in Fig. 7(b). With respect to base alloy (i.e., LM30), the overall dry sliding wear resistance of ITG-10, ITG10-T4, ITG10-T6 composites and cast iron has shown improvement by 38.40, 49.50, 52.86 and 50.56% (respectively) at 68.67 N applied load. While the wear resistance of ITG10-T4, ITG10-T6 composites and cast iron was enhanced by 16.70, 22.26 and 18.40% (respectively) with respect to ITG10 untreated sample. While these samples exhibited higher run-in wear loss as compared to cast iron which is surely associated to softer Al matrix than cast iron. Further, the lower density of the composite supports its applicability for brake rotors application as an alternate to cast iron.

3.5 Coefficient of Friction

The bar graph showing the coefficient of friction (COF) of Al-Si alloy (LM30), ITG10, ITG10-T4 and ITG10-T6 composite under different loading conditions and at same sliding distance are displayed in Fig. 8. The COF increased with increased applied load, as observed from Fig. 8. When the load is applied on the sample, pin asperity is in contact with counter disc asperity. During sliding motion, the asperity of the counter disc penetrates the pin surface with increasing load. This deep penetration of counter disc asperity requires more shear forces to continue the sliding movement. The resultant of this is the increased COF [49].

Furthermore, the COF of ITG10-T4 and ITG10-T6 dropped after the heat treatment of the prepared composite ITG10. The COF of ITG10 was reduced due to presence of hard ilmenite reinforcement and solid lubricants that resist the abrasive wear losses of the pin surface. The best result observed is for the ITG10-T6. A stable tribolayer was formed between the counter disc and pin surface. This tribolayer was able to reduce COF. The ITG10-T6 composites showed lower COF than the other samples. The COF of ITG10-T6 AMC was lower than ~ 53%, 16%, and 7% of LM30, ITG10 and ITG10-T4, respectively at 9.8 N load, shown in Fig. 8a. The COF of ITG10-T6 AMC was lower than ~ 54%, 29%, and 9% of LM30, ITG10 and ITG10-T4 (respectively) at 68.67 N load, shown in Fig. 8b.

3.6 Worn Surface and Debris Analysis

The morphology of the worn surfaces of ITG10-T4 and ITG10-T6 (at 9.81 and 68.67 N load) are displayed in Fig. 9(a, b) and 10(a, b), respectively. At a 9.81 N load,

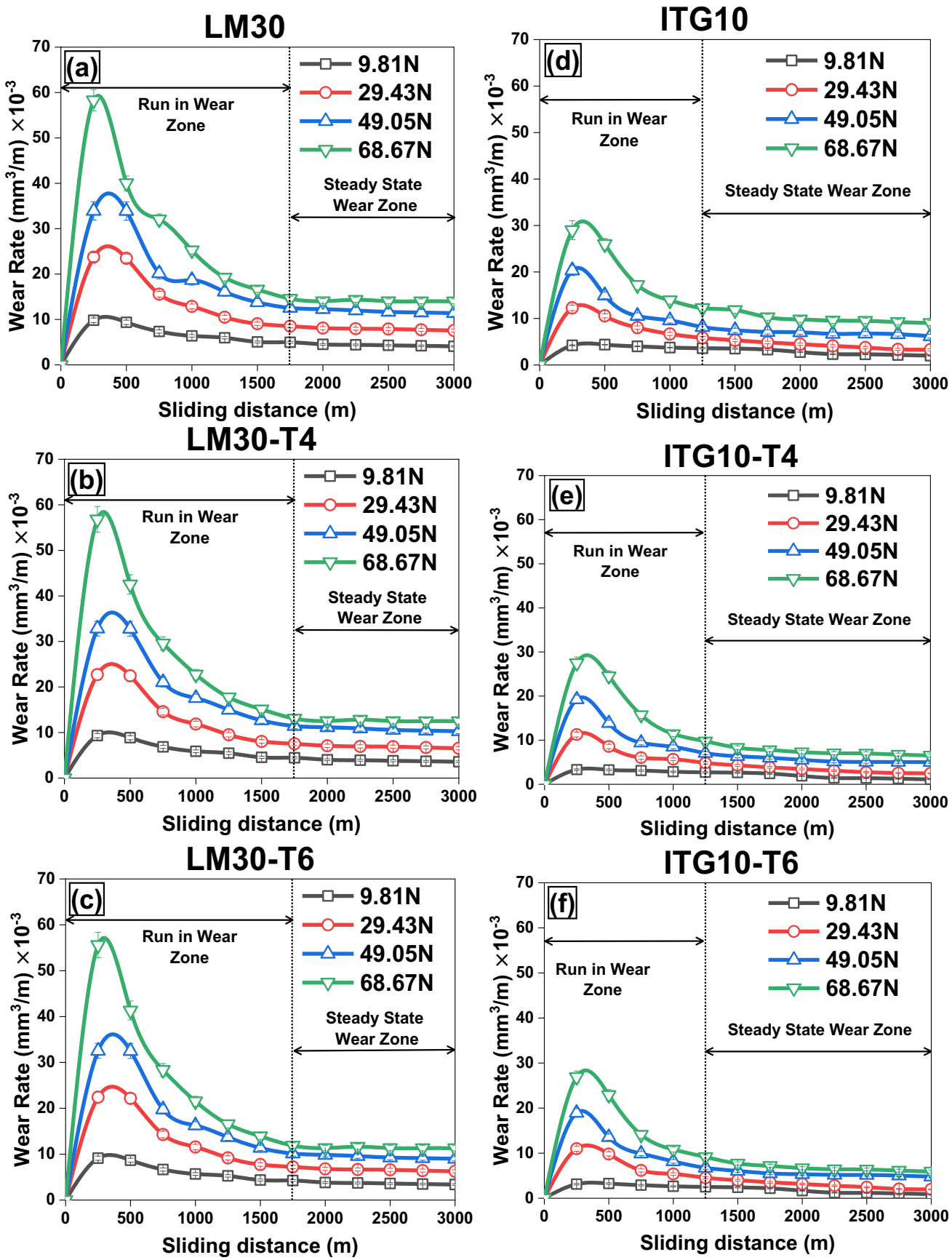
LM30
(a)
Run in Wear Zone
Steady State Wear Zone
9.81N
29.43N
49.05N
68.67N
Wear Rate (mm³/m) ×10⁻³
Sliding distance (m)
ITG10
(d)
LM30-T4
(b)
ITG10-T4
(e)
LM30-T6
(c)
ITG10-T6
(f)

◂**Fig. 6** Wear behavior of non-heat treated and heat-treated (T4, T6) alloy (LM30) and composite (ITG10) samples

the narrow grooves parallel to sliding direction with a small, delaminated surface area (Fig. 9a and 10a). These groves and craters (delaminated surface) indicate that the phenomenon was initiated by abrasion and delaminated wear mechanisms. Furthermore, micro debris on the worn surface suggested the entrapment of some debris between the sample and steel disc during sliding action as evidenced in the form of wide grooves shown in Fig. 9(b) and 10(b). Also, microcracks were observed (Fig. 10b) on the worn surface supported by the deformation of asperities under 68.67 N load. These micro-cracks further propagate and join each other leading to the material removal in the form of a sheet.

Further, SEM images of wear debris (at 9.81 and 68.67 N load) of ITG10-T4 and ITG10-T6 are shown in Fig. 9(c, d) and 10 (c, d), respectively. The debris significantly reduced the interaction of the soft matrix to the counter surface and worked as a load bearer, thus reducing the wear losses of synthesized composites. The

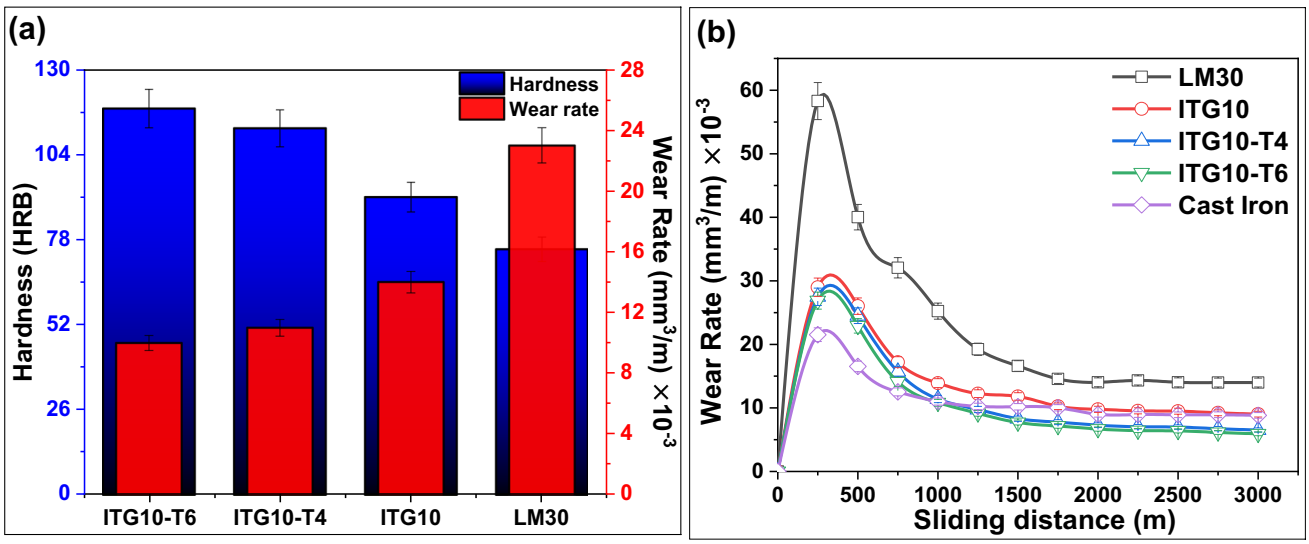

Fig. 7 (**a**) Relation between the hardness and wear rate, and (**b**) comparative wear graph of cast iron, non-heated, and heat-treated composite at 68.67 N load

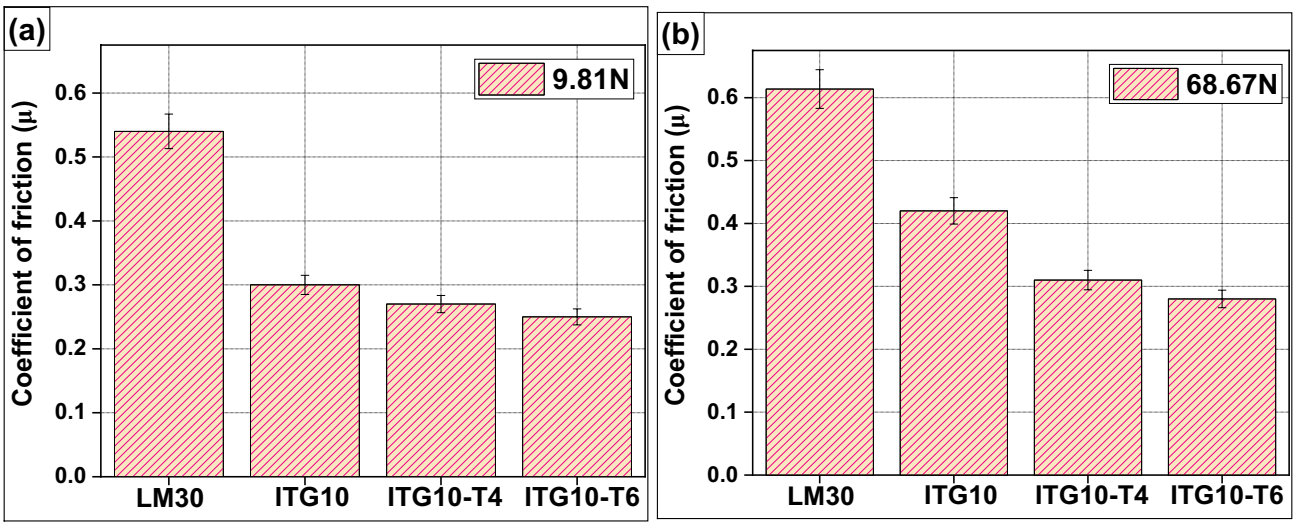

Fig. 8 Represents the coefficient of friction for prepared samples at (**a**) 9.81 N and (**b**) 68.67 N applied load

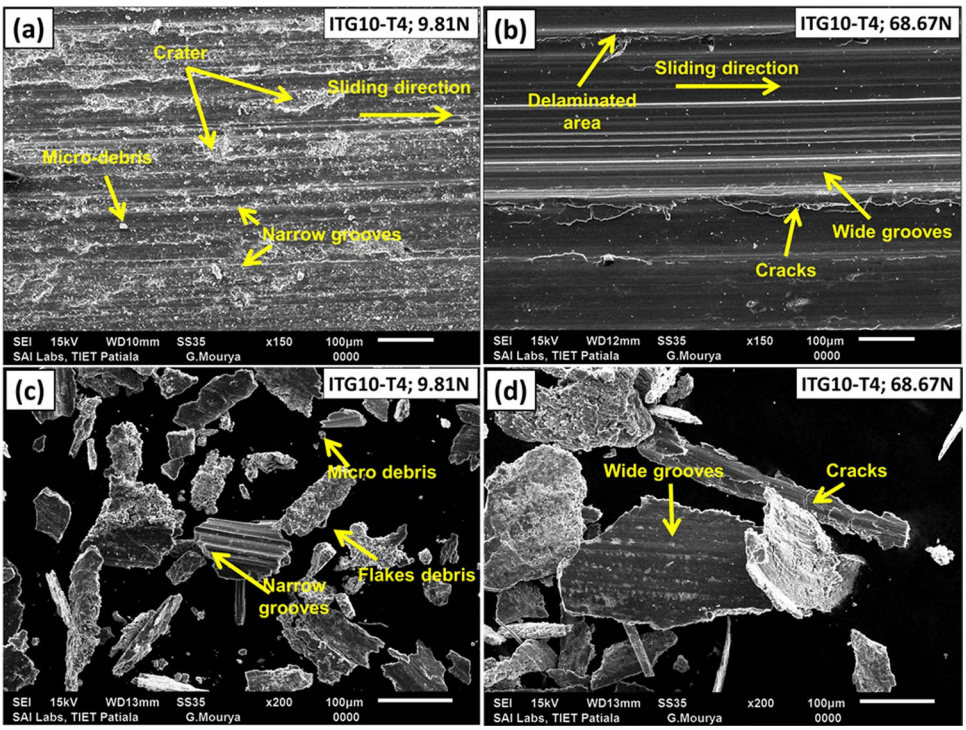

Fig. 9 SEM microstructure of (**a**, **b**) wear track and (**c**, **d**) debris of ITG10-T4 composite at low (9.81 N), and high (68.67 N) applied load

morphology of wear debris looked like flakes delaminated with detached ilmenite particles (Fig. 9c and 10c). These flakes are formed due to existing stress on the surface during continuous relative motion under applied loads [58]. Small flakes were produced by the crushing of bigger flakes under applied load containing wide grooves on the surface of the flakes due to cutting and micro-plowing action indicating the involvement of abrasive wear mechanism [34, 59]. Moreover, micro-cracks were also present on the delaminated flakes, as visible in Fig. 9(d) and 10(d), followed by adhesive wear mechanism.

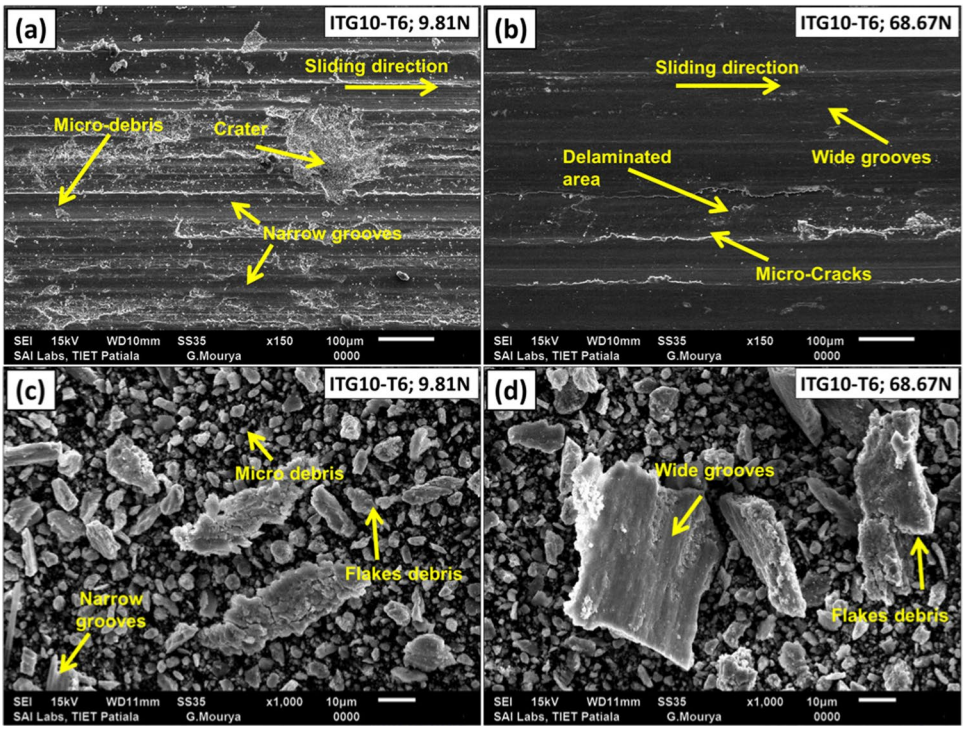

Fig. 10 SEM microstructure of (**a**, **b**) wear track and (**c**, **d**) debris of ITG10-T6 composite at low (9.81 N), and high (68.67 N) applied load

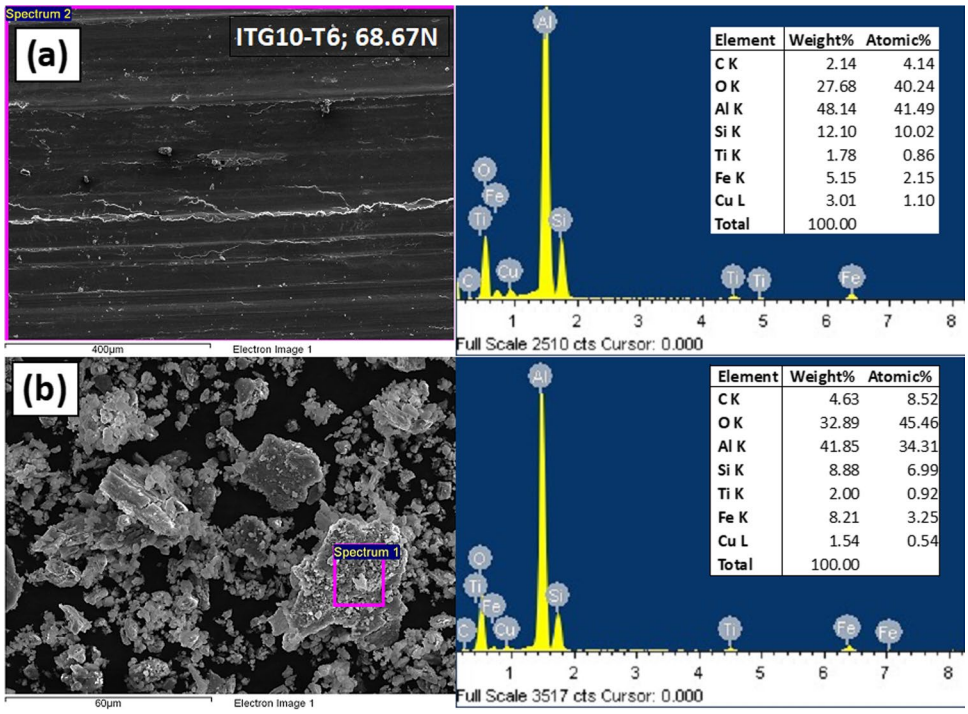

Fig. 11 EDS analysis of (**a**) wear track and (**b**) debris of ITG10-T6 sample at 68.67 N load

Figure 11(a) represents the EDS spectra of the wear track (ITG10-T6) under 68.67 N applied load. The chemical elemental analysis shows the presence of different elements like Al, Si, Fe, and O, etc. The presence of elemental oxygen confirmed the oxidation of the wear surface due to increasing contact temperature at high applied load. In this order, pin surface interacted with the steel counter surface leading to the transfer of Fe (from disc to prepared pin), forming a mechanically mix layer (MML) on the subsurface. This MML played a dynamic role in enhancing the wear resistance of synthesized composites

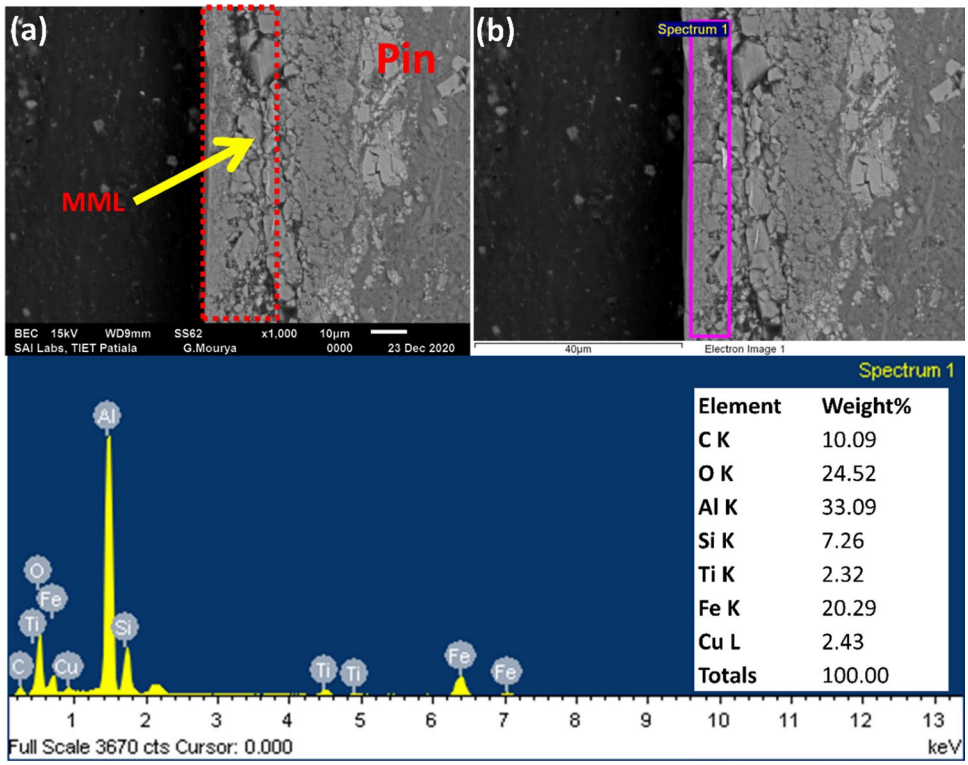

Fig. 12 Cross sectional study of ITG10-T6 wear track at 68.67 N load (**a**) SEM micrograph, and (**b**) EDS analysis

[60]. Consequently, the wear resistance of the ITG10-T6 was increased. Moreover, EDS results of wear debris, as shown in Fig. 11(b), supported the presence of elements on the worn out surface of ITG10-T6 under 68.67 N load. The spectrum shows the presence of O, Al, C, and Fe in wear debris. It shows that the abrasive wear mechanism was dominant in the beginning of sliding motion.

3.7 Cross Section Analysis

Figure 12(a) represent the cross-section analysis of wear track of ITG10-T6 sample. It revealed the presence of a compacted wear debris containing counter disc material, and various oxides in the tribolayer, due to continuous sliding motion and crushing action. There are few cracks observed under the wear track. The high hardness of the tribolayer (MML) reduces the transformation of shear force beneath the material. In addition, due to the formation of tribolayer, the transition in wear rate under continuous sliding also occurred. The EDS analysis of this tribolayer as shown in Fig. 12(b) confirms the presence of Al, O, Fe, and Si as major elements. Here, the presence of Fe indicated the transfer of counter disc material on the pin surface. Moreover, O indicates the formation of Al, Si, and Fe oxides during dry sliding of pin on counter surface.

4 Conclusion

The influence of heat treatment (tempering; T4 and T6) on the wear behavior of solid lubricants (Sn + Gr) and ilmenite reinforced LM30 composite has been successfully investigated. The key findings of the work are provided below.

- Refinement and redistribution of eutectic and primary Si was observed because of T4, and T6 heat treatment processes carried out on prepared ilmenite reinforced LM30 alloy composites.
- XRD pattern of heat-treated composite sample revealed the presence of Al, Si, and ilmenite as major constituents with some intermetallic phases ($FeSn_2$, Al_3Ti, Al_2Cu, $Al_{13}Fe_4$, FeTiSi and Mg_2Si).
- Maximum hardness of 112 HRB (due to redistribution of Si in metallic matrix) was obtained after 20 days of natural aging under T4 heat-treatment of prepared composite sample.
- Maximum hardness of 126 HRB was obtained after artificial aging at 180 °C for 4 h which got reduced to 117 HRB with increased heat treatment temperature (250 °C) under T6 heat-treatment.
- As an effect of tempering (T4 and T6), overall wear rate was improved by 16.69% and 22.20% as compared to ilmenite reinforced LM30 alloy (respectively) due to the formation of MML along with redistributed Si and ceramic particles. It is significantly higher than conventionally used cast iron, exhibiting 18.40% lower wear rate than ITG10 sample. Such considerable wear resistance of Al-composite sample would surely enable it as alternate material for brake drum applications.

Author's Contribution **Varun Singhal:** Conceptualization, design of study, data optimization, analysis, manuscript writing. **Aayush Gupta:** Conceptualization, data optimization, analysis, manuscript writing. **Om Prakash Pandey:** Results analysis, manuscript writing.

Data Availability All the data and material incorporated in the present manuscript will be made available whenever required.

Declarations

Formal consent is not compulsory for the above type of work.

Consent to Participate Authors does not perform any studies involving human or animal participation.

Consent for Publication Consent was got from all individual authors included in the study to publish data.

Conflict of Interest Authors do not have any conflict of interest.

References

1. Natarajan N, Vijayarangan S, Rajendran I (2006) Wear behaviour of A356/25SiCp aluminium matrix composites sliding against automobile friction material. Wear 261:812–822. https://doi.org/10.1016/j.wear.2006.01.011
2. Sharma V, Kumar S, Pandey OP (2012) Correlation of reinforced ceramicparticle's nature and size with microstructure and wear behavior of Al-Si alloy composite. Adv Mater Res 585:564–568. https://doi.org/10.4028/www.scientific.net/AMR.585.564
3. Garg T, Mathur P, Singhal V, Jain C, Gupta P (2014) Underwater Friction Stir Welding: An Overview. Int Rev Appl Eng Res 4:2248–9967
4. Rao BB (2018) Fabrication and mechanical behaviour of limonia acidissima ash – silicon carbide reinforced AL2024 alloy matrix hybrid composites. Int J Adv Res Ideas Innov Technol 4:1795–1802
5. Singh G, Goyal S (2018) Microstructure and mechanical behavior of AA6082-T6/SiC/B4C-based aluminum hybrid composites. Part Sci Technol 36:154–161. https://doi.org/10.1080/02726351.2016.1227410
6. Sharma S, Gupta R, Nanda T, Pandey OP (2021) Influence of two different range of sillimanite particle reinforcement on tribological characteristics of LM30 based composites under elevated temperature conditions. Mater Chem Phys 258:1–15. https://doi.org/10.1016/j.matchemphys.2020.123988
7. Alshmri F, Atkinson HV, Hainsworth SV, Haidon C, Lawes SDA (2014) Dry sliding wear of aluminium-high silicon hypereutectic alloys. Wear 313:106–116. https://doi.org/10.1016/j.wear.2014.02.010

8. Zhang J, Fan Z, Wang YQ, Zhou BL (2000) Microstructure and mechanical properties of in situ Al-Mg2Si composites. Mater Sci Technol 16:913–918. https://doi.org/10.1179/026708300101508685
9. Aravind M, Yu P, Yau MY, Ng DHL (2004) Formation of Al2Cu and AlCu intermetallics in Al(Cu) alloy matrix composites by reaction sintering. Mater Sci Eng A 380:384–393. https://doi.org/10.1016/j.msea.2004.04.013
10. Çelik A, Yaman H, Turan S, Kara A, Kara F, Zhu B et al (2018) Materials and surface engineering in tribology, vol 1, 1st edn, pp 1–223
11. Singhal V, Pandey OP (2021) Dry Sliding Wear Study of Solid Lubricants and Sillimanite-Reinforced Aluminum Alloy Composites. J Mater Eng Perform. https://doi.org/10.1007/s11665-021-05975-y
12. Arora R, Kumar S, Singh G, Pandey OP (2015) Effect of applied pressure on the tribological behaviour of dual particle size rutile reinforced LM13 alloy composite. Charact Miner Met Mater 2016:755–762. https://doi.org/10.1007/978-3-319-48191-3_95
13. Sharma SC (2001) The sliding wear behavior of A16061-garnet particulate composites. Wear 249:1036–1045. https://doi.org/10.1016/S0043-1648(01)00810-9
14. Kumar S, Panwar RS, Pandey OP (2012) Tribological characteristics of aluminium tri-reinforced particles (Al- TRP) composites developed by liquid metallurgy route. Adv Mat Res 585:574–578. https://doi.org/10.4028/www.scientific.net/AMR.585.57
15. Mohapatra S, Behera P, Das SK (2015) Heavy Mineral Potentiality and Alteration Studies for Ilmenite in Astaranga Beach. J Geosci Environ Prot 3:31–7
16. Singhal V, Pandey OP (2021) Wear and Friction Behavior of Gr/Sn Solid Lubricated Dual Reinforced AMCs. Silicon. https://doi.org/10.1007/s12633-021-01343-6
17. Karthikeyan S, Karunanithi R, Ghosh A (2021) Investigation on microstructures, mechanical and wear properties of Al 390/ZrO2 composite materials fabricated by P/M method. Multidiscip Model Mater Struct 17:149–166. https://doi.org/10.1108/MMMS-10-2019-0180
18. Mann VS, Pandey OP (2021) Influence of natural beach mineral corundum on the wear characteristics of LM30 aluminium alloy composites. Wear 477:203801. https://doi.org/10.1016/j.wear.2021.203801
19. Rasidhar L, Ramakrishna A, Rao CS (2013) Experimental Investigation on Mechanical Properties of Ilmenite based Al Nanocomposites. Int J Eng Sci Technol 5:1025–1030
20. Elwan M, Fathy A, Wagih A, Essa ARS, Abu-Oqail A, EL-Nikhaily AE (2019) Fabrication and investigation on the properties of ilmenite (FeTiO3)-based Al composite by accumulative roll bonding. J Compos Mater 54:1259–71. https://doi.org/10.1177/0021998319876684
21. Kumar CAV, Rajadurai JS (2016) Influence of rutile (TiO2) content on wear and microhardness characteristics of aluminium-based hybrid composites synthesized by powder metallurgy. Trans Nonferrous Met Soc China (English Ed) 26:63–73. https://doi.org/10.1016/S1003-6326(16)64089-X
22. Sarmadi H, Kokabi AH, Seyed Reihani SM (2013) Friction and wear performance of copper-graphite surface composites fabricated by friction stir processing (FSP). Wear 304:1–12. https://doi.org/10.1016/j.wear.2013.04.023
23. Edacherian A, Algahtani A, Tirth V (2018) Investigations of the tribological performance of A390 alloy hybrid aluminum matrix composite. Materials (Basel) 11:1–14. https://doi.org/10.3390/ma11122524
24. Singhal V, Prakash PO (2022) Study of wear losses and frictional heat dissipation during dry sliding wear of ilmenite reinforced Al-alloy composite. Proc Inst Mech Eng Part C J Mech Eng Sci 0:095440622110637. https://doi.org/10.1177/09544062211063782
25. Shanmugaselvam P, Sasikumar R, Sivaraj S. Investigation of Hardness and Tribological Behaviour of Aluminium Alloy LM30 Reinforced with Silicon Carbide, Boron Carbide and Graphite. Adv Manuf Technol, Springer Singapore; 2019, p. 569–76. https://doi.org/10.1007/978-981-13-6374-0_62
26. Sharma S, Nanda T, Pandey OP (2019) Investigation of T4 and T6 heat treatment on the wear properties of sillimanite reinforced LM30 aluminium alloy composites. Wear 426:27–36. https://doi.org/10.1016/j.wear.2018.12.065
27. Chen R, Iwabuchi A, Shimizu T (2000) The effect of a T6 heat treatment on the fretting wear of a SiC particle-reinforced A356 aluminum alloy matrix composite. Wear 238:110–119. https://doi.org/10.1016/S0043-1648(99)00328-2
28. Lashgari HR, Zangeneh S, Shahmir H, Saghafi M, Emamy M (2010) Heat treatment effect on the microstructure, tensile properties and dry sliding wear behavior of A356–10%B4C cast composites. Mater Des 31:4414–4422. https://doi.org/10.1016/j.matdes.2010.04.034
29. Singhal V, Pandey OP. Utilization of Natural Mineral Ilmenite-Reinforced Composites for the Dry Sliding Application. Int J Met. 2021;2. https://doi.org/10.1007/s40962-021-00724-2
30. ASM International Committee (1990) Heat treating of aluminum. In: ASM handbook, vol 4. Heat Treat, pp 841–879. https://doi.org/10.1361/asmhba000
31. Daoud AÃ, El-khair MTA, Abou El-khair MT (2010) Wear and friction behavior of sand cast brake rotor made of A359–20 vol% SiC particle composites sliding against automobile friction material. Tribol Int 43:544–553. https://doi.org/10.1016/j.triboint.2009.09.003
32. Shorowordi KM, Haseeb ASMA, Celis JP (2006) Tribo-surface characteristics of Al-B4C and Al-SiC composites worn under different contact pressures. Wear 261:634–641. https://doi.org/10.1016/j.wear.2006.01.023
33. Kumar S, Sharma V, Panwar RS, Pandey OP (2012) Wear behavior of dual particle size (DPS) zircon sand reinforced aluminum alloy. Tribol Lett 47:231–251. https://doi.org/10.1007/s11249-012-9983-y
34. Sharma V, Kumar S, Panwar RS, Pandey OP (2012) Microstructural and wear behavior of dual reinforced particle (DRP) aluminum alloy composite. J Mater Sci 47:6633–6646. https://doi.org/10.1007/s10853-012-6599-4
35. Sharma S, Nanda T, Pandey OP, Wire HAA, Parvizi AR, Hughes AE et al (2018) Effect of dual particle size (DPS) on dry sliding wear behaviour of LM30/sillimanite composites. Tribol Ind 123:142–154. https://doi.org/10.1016/j.diamond.2018.10.004
36. Panwar RS, Kumar S, Pandey R, Pandey OP, Singh R, Suresh P (2014) Study of non-lubricated wear of the Al-Si alloy composite reinforced with different ratios of coarse and fine size zircon sand particles at different ambient temperatures. Tribol Lett 55:83–92. https://doi.org/10.1007/s11249-014-0335-y
37. Singh M, Mondal DP, Das S (2006) Abrasive wear response of aluminium alloy–sillimanite particle reinforced composite under low stress condition. Mater Sci Eng A 419:59–68. https://doi.org/10.1016/j.msea.2005.11.056
38. Jorstad J, Apelian D (2009) Hypereutectic al-si alloys: Practical casting considerations. Int J Met 3:13–36. https://doi.org/10.1007/BF03355450
39. Chawla KK, Esmaeili AH, Datye AK, Vasudevan AK (1991) Effect of homogeneous/heterogeneous precipitation on aging behavior of SiCP Al 2014 composite. Scr Metall Mater 25:1315–1319. https://doi.org/10.1016/0956-716X(91)90407-R
40. Fathy A, El-Kady O, Mohammed MMM (2015) Effect of iron addition on microstructure, mechanical and magnetic properties of Al-matrix composite produced by powder metallurgy route.

Trans Nonferrous Met Soc China (English Ed) 25:46–53. https://doi.org/10.1016/S1003-6326(15)63577-4
41. Giefers H, Nicol M (2006) Equations of state of several iron-tin intermetallic compounds. J Phys Chem Solids 67:2027–2032. https://doi.org/10.1016/j.jpcs.2006.05.056
42. Singh G, Sharma N (2021) Study on the influence of T4 and T6 heat treatment on the wear behavior of coarse and fine WC particulate reinforced LM28 Aluminium cast composites. Compos Part C Open Access 4:100106. https://doi.org/10.1016/j.jcomc.2021.100106
43. Yılmaz O, Buytoz S (2001) Abrasive wear of Al_2O_3-reinforced aluminium-based MMCs. Compos Sci Technol 61:2381–2392
44. Surappa MK, Prasad SV, Rohatgi PK (1982) Wear and abrasion of cast Al-alumina particle composites. Wear 77:295–302
45. Panwar RS, Pandey OP (2013) Study of wear behavior of Zircon sand-reinforced LM13 alloy composites at elevated temperatures. J Mater Eng Perform 22:1765–1775. https://doi.org/10.1007/s11665-012-0383-0
46. Mohan S, Gautam G, Kumar N, Gautam RK, Mohan A, Jaiswal AK (2016) Dry sliding wear behavior of Al-SiO 2 composites. Compos Interfaces 23:493–502. https://doi.org/10.1080/09276440.2016.1149363
47. Singh M, Mondal DP, Jha AK, Das S, Yegneswaran AH (2001) Preparation and properties of cast aluminium alloy–sillimanite particle composite. Compos Part A Appl Sci Manuf 32:787–795
48. Makhatha ME, Fatoba OS, Akinlabi ET (2018) Effects of rapid solidification on the microstructure and surface analyses of laser-deposited Al-Sn coatings on AISI 1015 steel. Int J Adv Manuf Technol 94:773–787. https://doi.org/10.1007/s00170-017-0876-y
49. Gupta R, Sharma S, Nanda T, Pandey OP (2020) Wear studies of hybrid AMCs reinforced with naturally occurring sillimanite and rutile ceramic particles for brake-rotor applications. Ceram Int 46:16849–16859. https://doi.org/10.1016/j.ceramint.2020.03.262
50. Deuis RL, Subramanian C, Yellup JM (1996) Abrasive wear of aluminium composites - A review. Wear 201:132–144. https://doi.org/10.1016/S0043-1648(96)07228-6
51. Badia FA, Rohatgi PK (1969) Gall resistance of cast graphitic aluminum alloys. SAE Tech Pap. https://doi.org/10.4271/690275
52. Das S, Prasad SV, Ramachandran TR (1989) Microstructure and wear of cast (Al-Si alloy)-graphite composites. Wear 133:173–187
53. Tokisue H, Abbaschian GJ (1978) Friction and wear properties of aluminum-particulate graphite composites. Mater Sci Eng 34:75–78. https://doi.org/10.1016/0025-5416(78)90011-3
54. Gibson PR, Clegg AJ, Das AA (1984) Wear of cast Al-Si alloys containing graphite. Wear 95:193–198. https://doi.org/10.1016/0043-1648(84)90117-0
55. Giefers H, Nicol M (2006) High pressure X-ray diffraction study of all Fe-Sn intermetallic compounds and one Fe-Sn solid solution. J Alloys Compd 422:132–144. https://doi.org/10.1016/j.jallcom.2005.11.061
56. Tahiri H, Samuel AM, Doty HW, Valtierra S, Samuel FH (2018) Effect of Sr–Grain Refiner–Si Interactions on the Microstructure Characteristics of Al–Si Hypereutectic Alloys. Int J Met 12:307–320. https://doi.org/10.1007/s40962-017-0164-5
57. Annaiah MH, Gowda SL, Rajiv TG (2013) The Effect of Heat Treatment on the Microstructure, Mechanical Properties and Dry Sliding Wear Behaviour of a356O Reinforced. Int J Innov Res Sci Eng Technol 2(4):1038–42
58. Kumar S, Pandey R, Panwar RS, Pandey OP (2013) Effect of particle size on wear of particulate reinforced aluminum alloy composites at elevated temperatures. J Mater Eng Perform 22:3550–3560. https://doi.org/10.1007/s11665-013-0642-8
59. Kumar S, Panwar RS, Pandey OP (2013) Wear behavior at high temperature of dual-particle size zircon-sand-reinforced aluminum alloy composite. Metall Mater Trans A Phys Metall Mater Sci 44:1548–1565. https://doi.org/10.1007/s11661-012-1504-y
60. Venkataraman B, Sundararajan G (2000) Correlation between the characteristics of the mechanically mixed layer and wear behaviour of aluminium, Al-7075 alloy and Al-MMCs. Wear 245:22–38. https://doi.org/10.1016/S0043-1648(00)00463-4